JOURNAL OF Applied Polymer SCIENCE

Effect of Process Conditions on the Dart Impact Properties of Thin-Wall Injection-Molded Polycarbonate Plates

Jong-Sin Moon,[1] Jeong-Moo Lee,[1] Shi-Ho Lee,[1] Byoung-Ho Choi[2]

[1]Tech Center, LG Chem Ltd., 84 Jang-dong, Yuseong-gu, Daejeon 305-343, Republic of Korea

[2]School of Mechanical Engineering, Korea University, 1 5-ga, Anam-dong, Sungbuk-gu, Seoul 136-701, Republic of Korea

Correspondence to: B.-H. Choi (E-mail: bhchoi@korea.ac.kr)

ABSTRACT: Multifunctional mobile products, such as cellular phones, laptop computers, personal media players, etc., have become smaller and lighter; so the technology of thin-wall injection molding (TWIM) has been highlighted for making lightweight and compact mobile electronic products. Regarding mechanical properties, many portable electronic products should pass the so-called "drop test"; therefore, the evaluation of the dart (or impact) property of the housing that is made by the TWIM process is crucial for commercializing a product. However, extant research on the effect of injection molding process parameters on the physical properties of TWIM plates is insufficient as yet. Therefore, in this study, the pressure and temperature inside the cavity during the injection molding process are monitored by varying the injection molding process parameters, i.e., the gate size, injection speed, and melt temperature, and the effect of the average flow rate of the molten resin inside the cavity on the dart property of thin-wall injection-molded plates is examined. The dart property of thin-wall injection-molded plates is evaluated by the instrumented dart impact test to differentiate various responses of the load-displacement data during dart tests. © 2012 Wiley Periodicals, Inc. J. Appl. Polym. Sci. 000: 000–000, 2012

KEYWORDS: thin-wall injection molding; polycarbonate; instrumented dart impact

Received 31 March 2011; accepted 21 February 2012; published online

DOI: 10.1002/app.37549

INTRODUCTION

Multifunctional mobile products, such as cell phones, laptop computers, personal media players, etc., have become smaller and lighter; so, the technology of thin-wall injection molding (TWIM) has been highlighted for making lightweight and compact mobile electronic products. In general, a product that is less than 1 mm thick and with an aspect ratio (i.e., the ratio of the flow length to wall thickness) of more than 100 should be considered for applying TWIM.[1–3] TWIM is good for making lightweight products with a short cooling time and cost reduction, but fast solidification of the molten resin during TWIM can be an important practical issue. Hence, high speed and high pressure injection conditions are needed to decrease the time for filling molten resin in the mold, but such conditions are relatively too extreme to mold high quality product comparing with conventional injection molding (CIM). Therefore, precise process controls during TWIM are necessary to produce a thin-wall injection-molded product with satisfactory quality in comparison to CIM processes.

The required mechanical properties, such as the strength, stiffness, toughness, etc., of the thin-wall injection-molded housing of portable electronic products can be achieved by the optimization of the TWIM process of the product as well as the design optimization of the product and proper selection of the material. Therefore, an understanding of the structure–property–process relationship during the TWIM process is very important to develop a high-quality portable electronic product.

Research on TWIM has evaluated the mechanical properties by changing the injection molding process parameters similar to those for CIM. An understanding of the relationship between the injection molding process parameters and mechanical properties regarding the TWIM process is very important for modern portable electronic products, but only a few studies address this issue. Bushko and Stokes[4,5] studied the effect of injection molding process parameters on the shrinkage, warpage, and residual stresses of molded product. Liao et al.[6] reported the optimal process conditions of cellular phone housing by studying the stiffness of molded product considering geometric effects. Wang and Young[7] measured the residual stress of molded product under the layer removal method and studied the relationship between the observed residual stresses and the injection molding process conditions. Chen et al.[8] observed that

© 2012 Wiley Periodicals, Inc.

the mechanical properties of molded product are affected by residual stresses rather than by the flow-induced molecular orientation, and found that the reduction in the thickness of molded product and the increase in the injection speed can be important parameters for the formation of residual stresses. Chen et al.[9] investigated the relationship between the weld-line strength and injection molding process parameters. Chen et al.[10] also studied the dart property and flexural strength of the thin-walled housing of an electronic dictionary by using computer-aided engineering (CAE) analysis. Daiyan et al.[11,12] reported the low-velocity impact response of injection-molded polypropylene plates with some selected variables such as the striker geometry, clamping method, plate surface texture, melt flow weld lines, paint, and a couple of molding conditions (the molding temperature and holding pressure). They claimed that the occurrence of brittle fracture was affected by all the above factors except the molding conditions.

Especially regarding mechanical properties, many portable electronic products should pass the so-called "drop test"; therefore, an evaluation of the dart (or impact) property of the housing that is made by the TWIM process is crucial for commercializing a product. Engineers always try to keep the gate region as far away as possible from the likely regions of impact, but there are many reasons to locate the gate at a specific position. Extant research on the effect of injection molding process parameters on the dart properties of TWIM plates is insufficient as yet. Therefore, in this study, the pressure and temperature inside the cavity during the injection molding process are monitored by varying the injection molding process parameters, i.e., the gate size, injection speed, and melt temperature, and the effect of the average flow rate of the molten resin inside the cavity on the dart property of a thin-wall injection-molded plate is examined. The dart property of the plate is evaluated by an instrumented dart impact (IDI) test to differentiate various responses of the load-displacement data during dart tests.

MATERIALS AND OBSERVATION

Material and Test Specimens

The material used in this study is commercial-grade unfilled polycarbonate (PC), LUPOY SC-1004A from LG Chem, which is commonly used for the housing of portable electronic products because of its excellent impact properties. The physical properties of the test material are described in Table I. In Figure 1, the viscosity of tested sample is shown as a function of shear rate for three temperatures, 280, 300, and 320°C. Shear thinning effect is clearly observed at high rates of deformation. The dart specimen for IDI tests is a disk-shaped plate with diameter 100 mm and thickness 1.0 mm, as shown in Figure 2.

Table I. Physical Property of the Test Material

Properties	Unit	Standard	Value
Density	g/cm^3	ASTM D792	1.2
Melt flow rate	g/10 min	ASTM D1238	12
Tensile stress at yield	MPa	ASTM D638	56
Elongation to break	%	ASTM D638	100 <
Flexural strength	MPa	ASTM D790	88
Flexural modulus	MPa	ASTM D790	2100
Izod impact strength (notched)	kg·cm/cm	ASTM D256	70

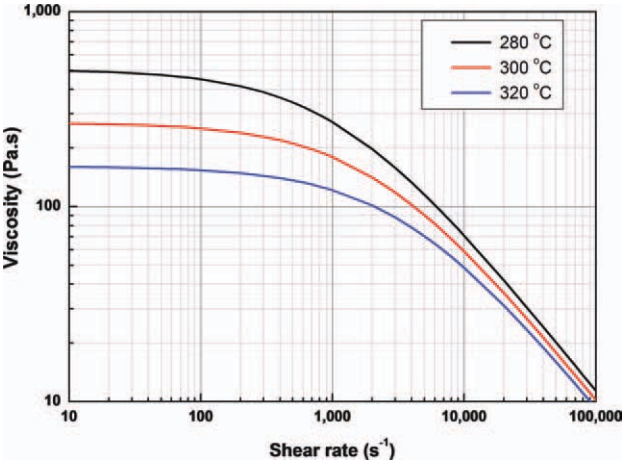

Figure 1. Viscosity curves for tested sample. [Color figure can be viewed in the online issue, which is available at wileyonlinelibrary.com.]

Injection Molding

A 140-ton high speed injection molding machine with 28 mm screw diameter from Sodic is used, and two melt temperatures (T), i.e., 300 and 320°C, and two injection speeds (v), i.e., 400 mm/s and 800 mm/s, are selected in this study. The mold temperature is 110°C, and the packing pressure is 88.2 MPa during the TWIM process. The packing time and cooling time are 1.5 s and 18 s, respectively. Proper packing and cooling time are determined by performing numerous pretests. A proper cooling time is selected by allowing sufficient time to solidify the injection molding product, and a proper packing time is determined by avoiding any short shot and/or sink mark on the product. The pin gate without an extruded hot nozzle is located at the center of the plate for a stable TWIM process, and three types of gate size (ϕ), i.e., 0.4, 0.6, and 0.8 mm (the gate sizes are

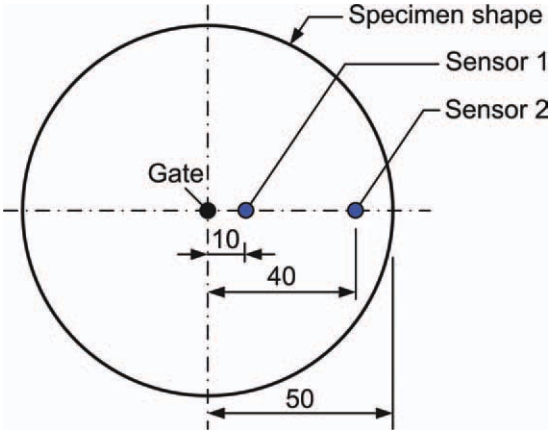

Figure 2. Center-gated disk specimen and location of the injection molding process monitoring sensor. [Color figure can be viewed in the online issue, which is available at wileyonlinelibrary.com.]

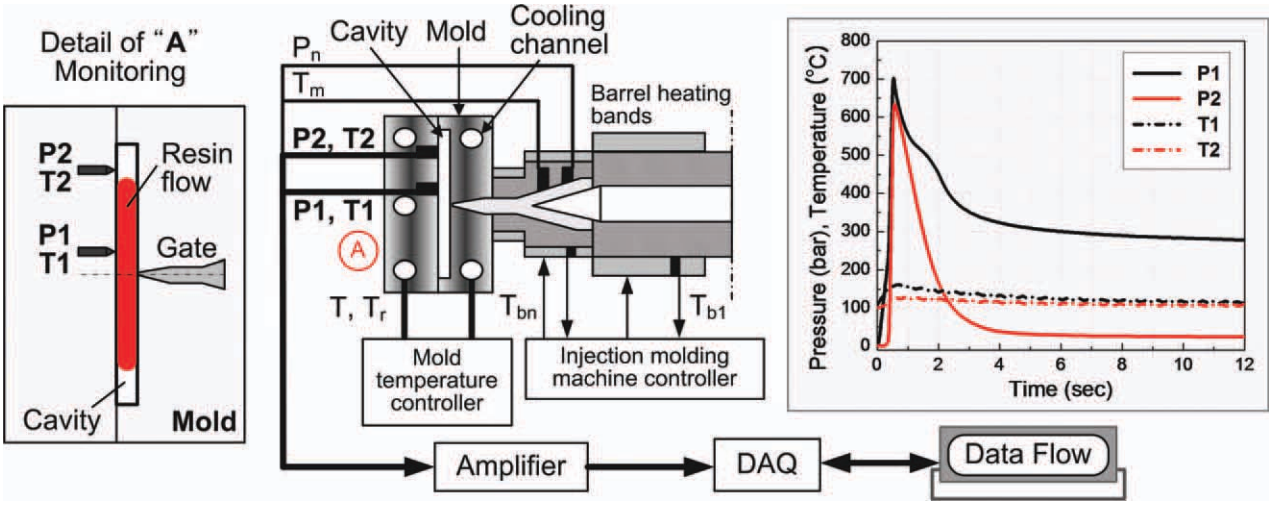

Figure 3. Hardware configuration of the monitoring system: the monitoring of pressure and temperature for injection process. [Color figure can be viewed in the online issue, which is available at wileyonlinelibrary.com.]

coded as G 0.4, G 0.6, and G 0.8, respectively), are considered for varying the shear rate during the TWIM process. We used pressure/temperature sensors 6910(CA) from Kistler for monitoring both pressure and temperature inside the cavity, and these sensors are installed 10 and 40 mm away from the center of the plate. The average flow rate of the molten polymer into the cavity is calculated by volume changes at a given time between sensors. In Figure 3, a schematic diagram of the hardware configuration of the monitoring system to monitor the pressure and temperature during the injection process is shown.

Instrumented Dart Impact Tests

The dart property of the plate is measured by IDI tests following ASTM D3763 and ISO 6603-2. The details of the evaluation and utilization of data provided by the IDI tests are described by Knakal and Ireland[13] for the above ASTM standard. The IDI tests are executed by Dynatup 9250Hv from INSTRON. The geometry of the striker (tup) is a hemisphere with diameter 12.7 mm. The clamping methods and impact locations are varied as shown in Figure 4. Two types of clamping ring with diameters of 40 mm and 80 mm, respectively, are used (the clamping-ring diameters are coded as C40 and C80, respectively), and two types of impact location, i.e., the center of the plate and 20 mm from the center (coded as CI and OI, respectively) are considered. The impact energy and impact velocity are selected based on preliminary tests for various plate types to ensure complete penetration during the IDI tests, i.e., 14 J and 2.0 m/s for the CI specimen and 24 J and 2.7 m/s for the OI specimen. A summary of the injection molding conditions and the IDI test conditions is shown in Table II.

TEST RESULTS

Weight Variation of Injection-Molded Specimens

The weight of each injection-molded specimen is measured to monitor the variation of injection-molded specimens during the injection molding process so that it is possible to check the stability of the injection molding process. In Figure 5, the measured weights of the injection-molded specimens are shown. For each injection molding condition, 50 specimens are weighted.

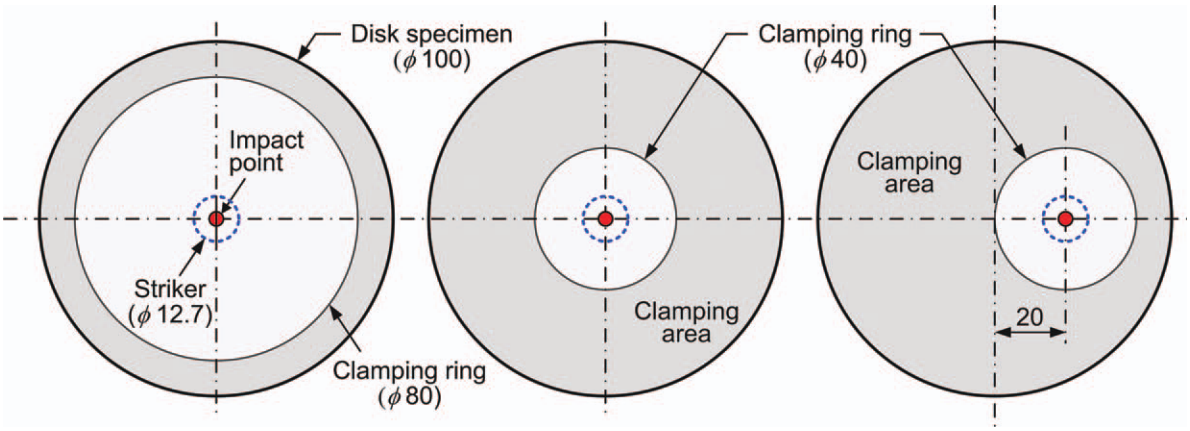

Figure 4. Impact test conditions: different clamping size/location and impact point of disk specimen. [Color figure can be viewed in the online issue, which is available at wileyonlinelibrary.com.]

Applied Polymer SCIENCE

Table II. Specimen (Gate Size), Injection Mold Condition, and Impact Test Condition

Gate size	Injection mold condition		Impact test condition		
Diameter (mm)	Temperature (°C)	Speed (mm/s)	Impact position	Clamping dia. (mm)	Specimen code
0.4	300	400	Center	80	CI (C80)
0.6	320	800	Center	40	CI (C40)
0.8	-	-	Offset	40	OI (C40)

In general, it can be observed that the weight of a specimen increases as the gate size increases. This is because of the uniform transmission of the pressure to the molten resin, which could be confirmed by monitoring pressure sensors during the injection molding process. Interestingly, specimens molded at low temperature (300°C) are heavier than specimens molded at high temperature (320°C) possibly because the melt density of the resin at low temperature is higher than that at high temperature. Kamal et al.[14] reported the weight of a part is a nonlinear function of the bulk temperature and the cavity pressure. The effect of the injection speed on the weight variation of the injection-molded specimens is not clearly identified for our experiments.

A statistical summary of the weight variation is shown in Table III. The difference between the maximum weight (specimens molded at $\phi = 0.8$ mm, $T = 300$°C, and $v = 400$ mm/s) and the minimum weight (specimens molded at $\phi = 0.4$ mm, $T = 320$°C, and $v = 400$ mm/s) is ~ 0.18 g. In addition, for the same process condition, the weight variation is very small so that it can be ascertained that the injection molding process is very stable for each condition.

Variation of the Cavity Pressures During the Injection Molding Process

In Figure 6, the variation of the cavity pressures measured from two sensors during the injection molding process is shown. By comparing the profiles of the cavity pressure from two sensors, many injection molding characteristics, such as the filling time of the molten resin, the actual flow rate, the actual injection speed, and so on, can be analyzed. As shown in Figure 6(a), profiles of the cavity pressure measured at the two sensors are clearly different, and three phases can be identified from the profiles, i.e., an injection phase, a compression phase, and a holding pressure phase.

In Figure 6(b), profiles of the cavity pressure measured for two injection speeds at the two sensors are shown, and the effect of

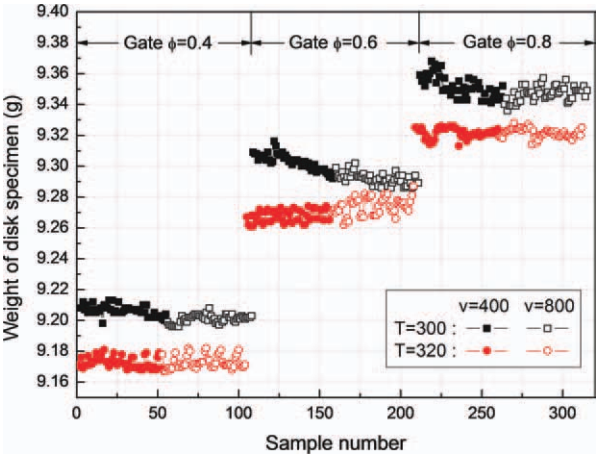

Figure 5. Measured shot-to-shot weight diagram of injection-molded specimens. [Color figure can be viewed in the online issue, which is available at wileyonlinelibrary.com.]

the injection speed on the profile of the cavity pressure is not clearly observed. This is possibly because the viscosity of the test material (PC) is relatively high and the flow resistance of PC increases so that the variation of the injection speed from 400 mm/s to 800 mm/s is not very effective for differentiating profiles of the cavity pressure. Stevenson et al.[15] observed a similar trend between the cavity pressure and injection rate; their explanation was that a complicated viscous characteristics of the resin flow cause an inverse relationship between the viscosity and the flow rate with the result that the cavity pressure is nearly independent of Q. Both the actual injection speed and the actual flow rate increase linearly when the gate size increases. As the gate size increases, the pressure loss around the gate decreases so that the flow rate and injection speed increase.

As shown in Figure 6(c,d), the measured cavity pressures at the two sensors ($P1$ and $P2$) increase and the difference in cavity pressure between the two sensors ($\Delta P = P1 - P2$) decreases when the gate size is increased. As the melt temperature increases, the difference in cavity pressure between the two sensors decreases more. Therefore, when the gate size increases, additional molten resin can enter the cavity under higher pressure. Hence, the melt density and the weight of the specimen increase together eventually. As the melt temperature increases from 300 to 320°C, the variation of the cavity pressure afar from the gate ($P2$) is much larger than that near the gate ($P1$). Hence, the actual injection speed and the actual flow rate increase together; this is caused by a reduction in the viscosity of the molten resin, i.e., an increase in the flowability.

Table III. Part Weight with Different Process Conditions [unit (g)]

	Gate(mm)	$\phi = 0.4$		$\phi = 0.6$		$\phi = 0.8$	
Temperature (°C)	Speed(mm/s)	$v = 400$	$v = 800$	$v = 400$	$v = 800$	$v = 400$	$v = 800$
$T = 300$	Mean	9.2063	9.2009	9.3025	9.2918	9.3512	9.3469
	STDEV	0.0032	0.0027	0.0052	0.0037	0.0069	0.0048
$T = 320$	Mean	9.1728	9.1729	9.2674	9.2740	9.3215	9.3214
	STDEV	0.0037	0.0041	0.0039	0.0055	0.0032	0.0028

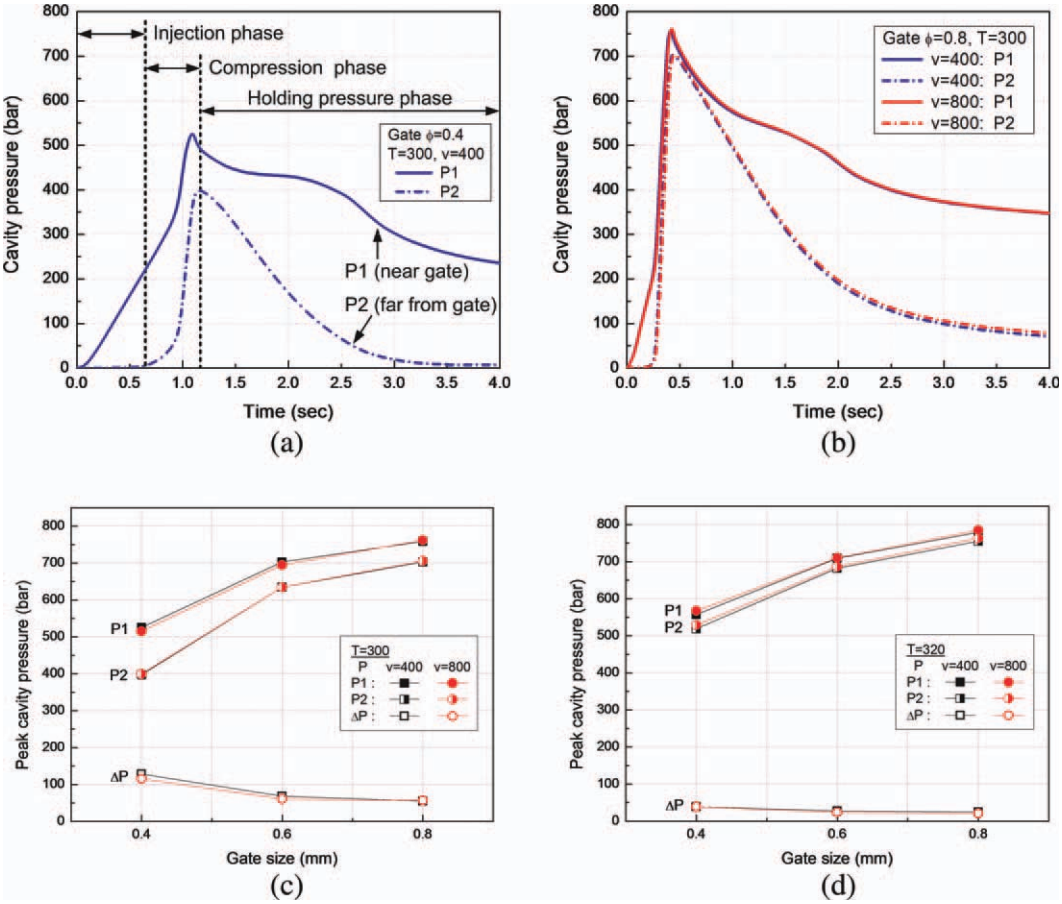

Figure 6. Variation of the cavity pressures measured from two sensors during injection molding process. (a) G 0.4, $T = 300°C$, $v = 400$ mm/s. (b) G 0.8, $T = 300°C$. (c) $T = 300°C$. (d) $T = 320°C$. [Color figure can be viewed in the online issue, which is available at wileyonlinelibrary.com.]

In Table IV, the average melt flow rate in the cavity is summarized. The average melt flow rate is calculated by the arrival time of the molten resin between sensors. The average melt flow rate of the molten resin increases in proportion to the gate size, i.e., the average flow rate increases by only ~ 10% as the injection speed doubles (from 400 mm/s to 800 mm/s); therefore, it can be seen that the effect of the injection speed on the flow rate is not significant. As the melt temperature increases from 300 to 320°C, the average flow rate approximately doubles. Therefore, it can be confirmed that the gate size and melt temperature can be dominant factors for controlling the average flow rate and the shear rate in the cavity. As shown in the next section, there is a strong relationship between the average flow rate, i.e., flow-induced shear orientation, and IDI properties. Some additional experiments and simulations to understand the precise movements of the molten resin and the pressure/shear stress fields in the cavity during injection molding process can be helpful to clarify observations in this study in the future.

Variation of the Dart Impact Property

Force-Deflection Curve. In Figure 7, force-deflection curves obtained by the IDI tests with variable sample conditions, i.e., the impact location, the size of the clamping ring, and injection molding conditions, are shown. As shown in Figure 7, initially, the curve is relatively linear (elastic) and then shows nonlinear behavior up to the peak load. The linear slope of the initial force-displacement curve is referred as the relative stiffness. After the peak point is passed, the samples are broken with regard to two types of failure mechanism, i.e., radial crack growth with limited elongation (tearing failure) and circumferential crack

Table IV. Average Melt Flow Rate in the Cavity Based on the Arrival Time Between Sensors

	Gate(mm)	ϕ = 0.4		ϕ = 0.6		ϕ = 0.8	
Temperature (°C)	Speed(mm/s)	v = 400	v = 800	v = 400	v = 800	v = 400	v = 800
T = 300	Time (s)	0.522	0.485	0.275	0.253	0.193	0.191
	Flow rate (cm^3/s)	9.03	9.71	17.13	18.59	24.43	24.67
T = 320	Time (s)	0.250	0.240	0.124	0.113	0.099	0.085
	Flow rate (cm^3/s)	18.88	19.60	38.05	41.67	47.49	55.19

Applied Polymer SCIENCE

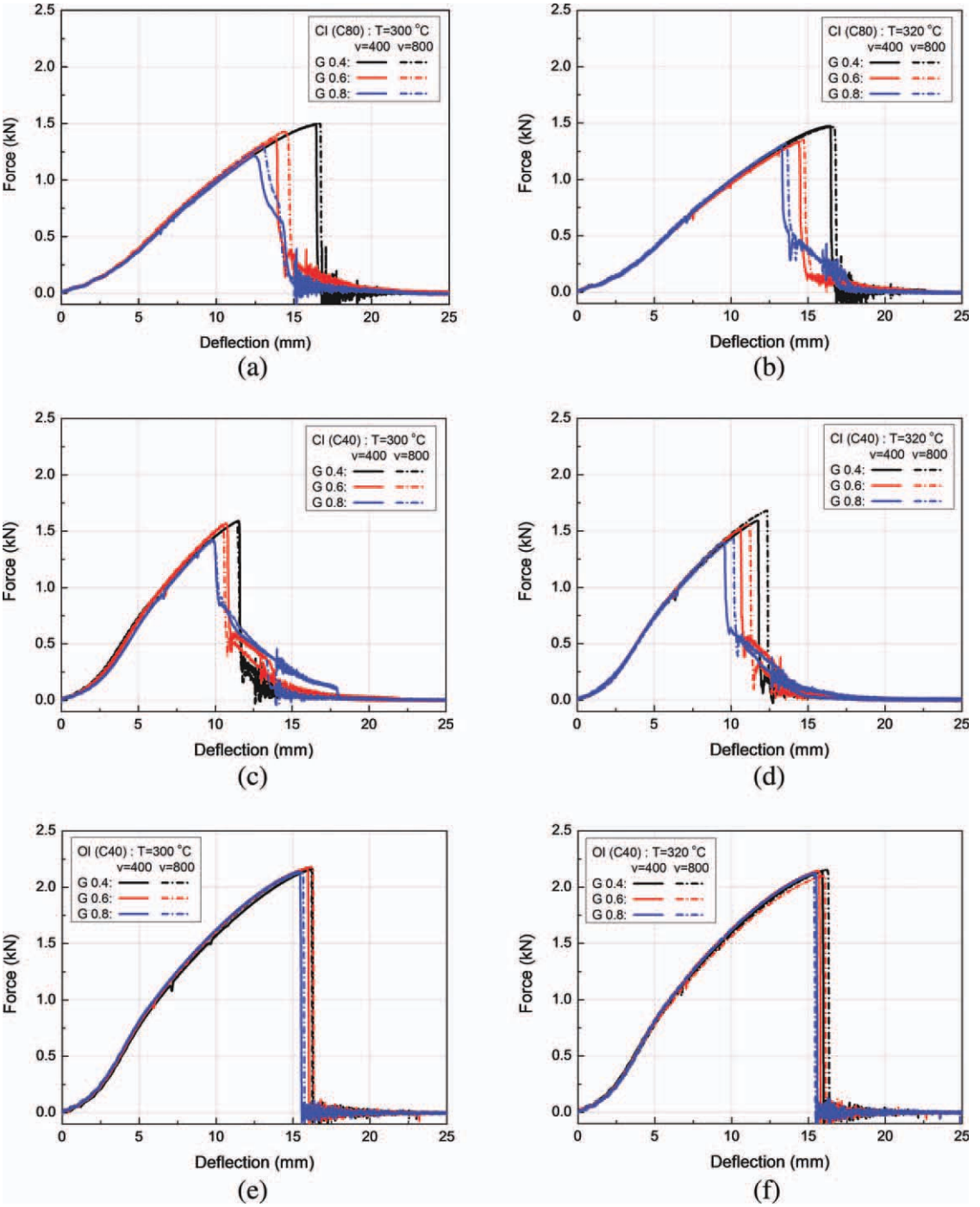

Figure 7. Force-deflection curves with different injection molding condition. (a) CI (C80), $T = 300°C$. (b) CI (C80), $T = 320°C$. (c) CI (C40), $T = 300°C$. (d) CI (C40), $T = 320°C$. (e) OI (C40), $T = 300°C$. (f) OI (C40), $T = 320°C$. [Color figure can be viewed in the online issue, which is available at wileyonlinelibrary.com.]

growth with large elongation (button-like failure). The difference in failure mechanism will be discussed later in this subsection.

Both the peak load and the maximum deflection increase as the gate size decreases. As shown in Figure 7(a–d), the effect of the gate size is clearer when the large clamp ring (C80) is used. Because the amount of deflection is limited in the case of the small clamp ring, both the relative stiffness and the peak load increase, but the deflection at the peak load decreases so that the total impact energy decreases. In the case of the CI (C80) samples, the failure mechanism is affected by the gate size, i.e., the G 0.4 samples are broken with circumferential crack growth and large elongation (button-like failure) and the G 0.8 samples are broken with radial crack growth and limited elongation (tearing failure) in general. In the case of the CI (C40) samples,

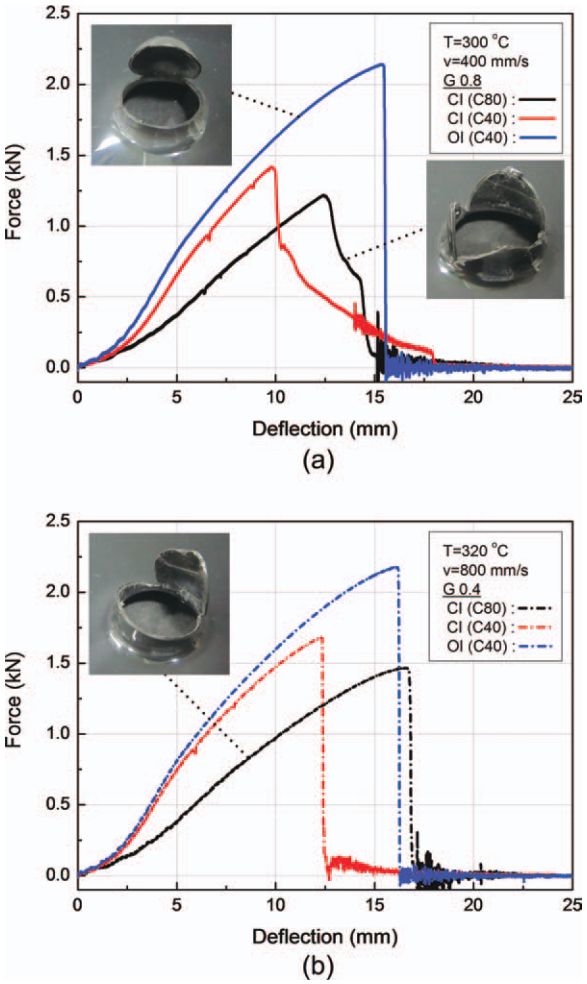

Figure 8. Force-deflection curves with different impact striking condition. (a) $T = 300°C$, $v = 400$ mm/s, G 0.8. (b) $T = 320°C$, $v = 800$ mm/s, G 0.4. [Color figure can be viewed in the online issue, which is available at wileyonlinelibrary.com.]

most samples are broken with radial crack growth and limited elongation regardless of the gate size; this may be related to the limited deflection due to the small clamping size.

As shown in Figure 7(c–f), the effect of the impact location on the peak load is clearly seen regardless of the injection molding conditions. The relative stiffness of the CI and OI samples is not that different for the same clamp ring size, but the peak load is very different, i.e., the OI samples show higher peak loads than the CI samples. Hence, the total impact energy of the OI samples is larger than that of the CI samples. Also, it can be noticed that an abrupt drop in the load after the peak load passed is observed in the case of the OI samples, viz., those with circumferential crack growth and large elongation. The effect of the gate size on the relative stiffness is very limited, but the effect of the clamping-ring size on the relative stiffness can be observed clearly, as shown in Figure 8.

As shown in Figure 7, the force-displacement behavior is affected by the heterogeneity of the gate region during the injection molding process. Especially, by comparing the force-displacement curves of the CI and OI samples with the same clamp ring size (C40), the relative stiffness is seen to be similar but the overall force-displacement behavior is obviously different (the difference in the impact energy is recorded as being up to 25–35%). Daiyan et al.[12] observed similar behavior for another kind of source of the heterogeneity of injection-molded product, viz., melt flow weld lines. They reported that the absorbed dart impact energy of a plate with a weld line was significantly reduced compared with those of plates without a weld line. Therefore, it can be understood that gate design for injection-molded products is very important. Hence, the major factors for controlling the dart impact property can be the gate size and the gate location rather than the injection-molding conditions such as the melt temperature, injection speed, and so on. A detailed analysis of the effect of the gate size and location on the dart property is rather complicated and under study as a separate work using residual stresses and orientation studies as well as morphological analyses of specimens.

Variation of Parameters from Dart Impact Tests. As mentioned above, the gate size can be an important factor for controlling the dart impact behavior; hence, the effect of the gate size on the parameters of the dart impact test is analyzed in detail. The variation of the parameters, i.e., the peak load and the total absorbed energy, regarding the dart impact test is shown with variable gate sizes in Figure 9.

As shown in Figure 9(a,c,e), in the case of the CI samples, the peak load decreases as the gate size increases, but in the case of the OI samples, the peak load is not affected by the gate size in general (less than 1%). The difference between the peak loads of G 0.4 and G 0.8 for the CI (C40) and CI (C80) samples is ~ 11–16%.

As shown in Figure 9(b,d,f), the total absorbed energy decreases as the gate size increases. Interestingly, compared with the OI samples, the CI samples show a large variation in the total absorbed energy (up to 30% for the C80 samples and up to 20% for the C40 samples); also, it can be observed that the tailored force-displacement behavior after the peak load of the CI samples is more varied than that of the OI samples. Hence, the tailored force-displacement behavior after the peak load can be important for the variation of the total absorbed energy unless the sample is extremely brittle. Also, the change in the failure mechanism should be considered to explain the variation of the total absorbed energy, i.e., the failure mechanism of the CI (C80) samples is changed from circumferential crack growth with large elongation to radial crack growth with limited elongation. It can be known that the total absorbed energy in the case of circumferential crack growth and large elongation is larger than that in the case of radial crack growth and limited elongation. In the case of the OI samples, the effect of the gate size on the total absorbed energy is relatively small (less than 8%) and the failure mechanism is the same in all cases, i.e., circumferential crack growth with large elongation.

CONCLUSION

In this study, the pressure and temperature inside the cavity during the injection molding process are monitored by varying the injection molding process parameters, i.e., the gate size,

Applied Polymer SCIENCE

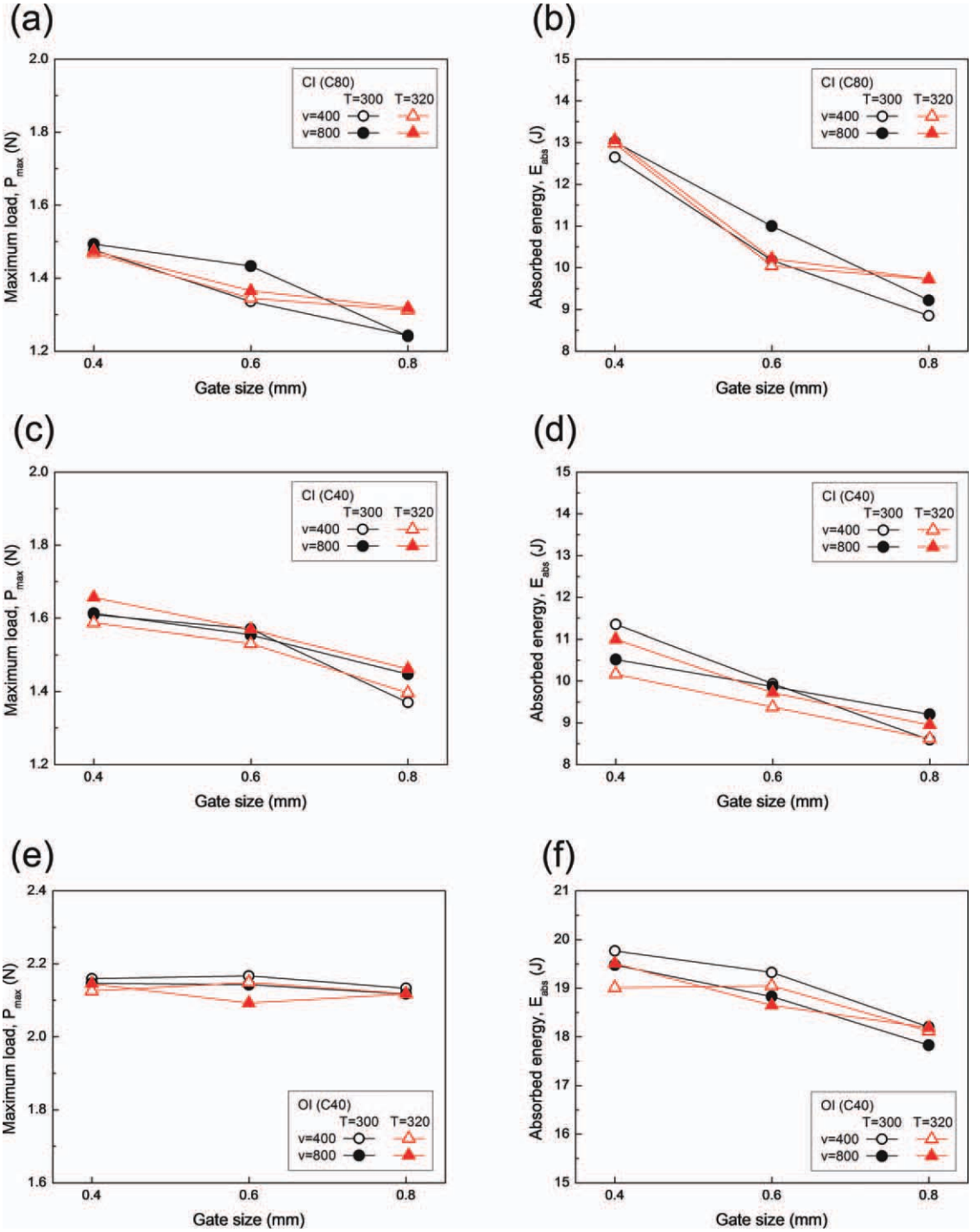

Figure 9. The variation of impact properties with gate size (a) Maximum load, P_{max} [CI(C80)]. (b) Total absorbed energy, E_{abs} [CI(C80)]. (c) Maximum load, P_{max} [CI(C40)]. (d) Total absorbed energy, E_{abs} [CI(C40)]. (e) Maximum load, P_{max} [OI(C80)]. (f) Total absorbed energy, E_{abs} [OI(C80)]. [Color figure can be viewed in the online issue, which is available at wileyonlinelibrary.com.]

injection speed, and melt temperature, and the dart property of the plate is evaluated by an IDI test to differentiate various responses in the load-displacement data during the dart tests. Here is a summary of the study.

1. It can be observed that the weight of a specimen increases as the gate size increases due to uniform transmission of the pressure to the molten resin, and, interestingly, the weight of a specimen increases slightly as the melt temperature increases from 300 to 320°C. However, the effect of the injection speed on the weight variation of injection-molded specimens is not clearly identified.
2. The actual injection speed and the actual flow rate increase linearly as the gate size increases. In addition, as the gate size increases, the pressure loss around the gate

decreases so that the flow rate and injection speed increase. So, it can be confirmed that the gate size and melt temperature can be dominant factors for controlling the average flow rate and the shear rate in the cavity.

3. The average melt flow rate of the molten resin increases in proportion to the gate size. As the melt temperature increases from 300 to 320°C, the average flow rate approximately doubles; this is caused by a reduction in the viscosity of the molten resin, i.e., an increase in the flowability. Hence, it can be known that the gate size and melt temperature can be dominant factors for controlling the average flow rate in the cavity.
4. Both the peak load and the maximum deflection increase as the gate size decreases, and it is clearly observed that the impact location affects the peak load. The major factors for controlling the dart impact property can be the gate size and the gate location rather than injection molding conditions such as the melt temperature, injection speed, and so on. Compared with the OI samples, the CI samples show a large variation in the total absorbed energy due to a large variation in the tailored force-displacement behavior after the peak load. Also, the change in the failure mechanism should be considered to explain the variation in the total absorbed energy.

REFERENCES

1. Tantakom, P.; Schott, N. R. In Proceedings of SPE/ANTEC 98, Atlanta, USA, April 26–30, 1998; CRC Press: Brookfield, **1998.**
2. Shen, Y. K.; Yeh, P. H.; Wu, J. S. *Int. Commun. Heat Mass Transf.* **2001,** *28*, 1035.
3. Shelden, R. *J. Inject. Mold. Technol.* **2000,** *3*, 159.
4. Bushko, W. C.; Stokes, V. K. *Polym. Eng. Sci.* **1995,** *35*, 351.
5. Bushko, W. C.; Stokes, V. K. *Polym. Eng. Sci.* **1996,** *36*, 322.
6. Liao, S. J.; Chang, D. Y.; Tsou, H. J.; Ho, J. R.; Yau, H. T.; Hsieh, W. H.; Wang, J. T.; Su, Y. C. *Polym. Eng. Sci.* **2004,** *44*, 917.
7. Wang, T.; Young, W. *Eur. Polym. J.* **2005,** *41*, 2511.
8. Chen, S.-C.; Peng, H.-S.; Huang, L.-T.; Chung, M.-S. *J. Reinforce. Plast. Compos.* **2003,** *22*, 479.
9. Chen, C.-S.; Chen, T.-J.; Chien, E.-D.; Chen, S.-C. *Int. Commun. Heat Mass. Transf.* **2007,** *34*, 448.
10. Chen, S. C.; Wang, H. I.; Chen, J. P.; Peng, H. S. *J. Appl. Polym. Sci.* **2002,** *86*, 3064.
11. Daiyan, H.; Andreassen, E.; Grytten, F.; Lyngstad, O. V.; Luksepp T.; Osnes H. *Polym. Test* **2010,** *29*, 648.
12. Daiyan, H.; Andreassen, E.; Grytten, F.; Lyngstad, O. V.; Luksepp T.; Osnes H. *Polym. Test* **2010,** *29*, 894.
13. Knakal, W.; Ireland, D. R. In Instrumented Impact Testing of Plastics and Composite Materials, ASTM STP 936; Kessler, S. L., Adams, G. C., Driscoll, S. B., Ireland, D. R., Eds.; American Society for Testing and Materials: Philadelphia, **1987;** p 44.
14. Kamal, M. R.; Varela, A. E.; Patterson, W. I. *Polym. Eng. Sci.* **1999,** *39*, 940.
15. Stevenson, F.; Galskoy, A.; Wang, K. K.; Chen, I.; Reber, D. H. *Polym. Eng. Sci.* **1977,** *17*, 706.